Optical properties of nanotubes / Propriétés optiques des nanotubes

Infrared sensors based on multi-wall carbon nanotube films

Senseurs infrarouges à base de couches minces de nanotubes de carbone multi-parois

Philippe Mérel [a,*], Jean-Baptiste Anumu Kpetsu [b], Charlie Koechlin [c], Sylvain Maine [c], Riad Haidar [c], Jean-Luc Pélouard [d], Andranik Sarkissian [b], Mihnea Ioan Ionescu [e], Xueliang Sun [e], Philips Laou [a], Suzanne Paradis [a]

[a] DRDC Valcartier, 2459, boulevard Pie-XI, Québec, Québec, Canada G3J 1X5
[b] Plasmonique Inc. 9092 Rimouski, Brossard, Québec, Canada J4X 2S3
[c] Le centre français de recherche aérospatiale ONERA, chemin de la Hunière, 91761 Palaiseau cedex, France
[d] Laboratoire de photonique et de nanostructures du CNRS, route de Nozay, 91460 Marcoussis, France
[e] University of Western Ontario, Department of Mechanical and Materials Engineering, London, Ontario, Canada N6A 5B9

A R T I C L E   I N F O

A B S T R A C T

In order to fabricate novel infrared sensors, dense films of multi-wall carbon nanotubes have been grown on silicon and alumina substrates, using Plasma enhanced Chemical Vapour Deposition technique. The physical and optical characteristics of the devices were studied using a variety of methods. The carbon nanotube on silicon device showed a peak response at a wavelength of 1.02 µm. The infrared response of the carbon nanotube on alumina device showed that the detection behavior was consistent with a bolometric effect. Measurements have also revealed a wide spectral response from the visible to the long-wave infrared for that sample.

© 2010 Published by Elsevier Masson SAS on behalf of Académie des sciences.

R É S U M É

Des couches denses de nanotubes de carbone multi-parois ont été synthétisées par un procédé plasma sur des substrats de silicium et d'alumine dans le but de fabriquer un nouveau type de capteur infrarouge. Les propriétés physiques et optiques des dispositifs ont été étudiées grâce à diverses méthodes. Les dispositifs à base de nanotubes sur silicium démontrent une réponse infrarouge maximum à une longueur d'onde de 1,02 µm. La réponse infrarouge des dispositifs de nanotubes sur alumine peut être expliquée par un effet bolométrique. Il est aussi déterminé que la réponse spectrale de cet échantillon s'étend du visible à l'infrarouge lointain.

© 2010 Published by Elsevier Masson SAS on behalf of Académie des sciences.

1. Introduction

Infrared imaging capability is a major tool of modern defense organizations. It is a critical capability for many operations; from dismounted soldier portable systems to more complex airborne systems installed on unattended air vehicles. The different wavelength bands of interest for defense and security can be divided in the following way and are, to a large

extent, defined by atmospheric transmission considerations: near-infrared (0.7 μm to 1 μm), short-wavelength infrared (1 μm to 3 μm), mid-wavelength infrared (3 μm to 5 μm) and long-wavelength infrared (8 μm to 12 μm). For each of these bands, many sensing technologies are used to perform imaging. If we focus on the long-wavelength infrared band, we can identify two main sensing technologies that present very different characteristics. First, mercury–cadmium–telluride (MCT) systems use this small band-gap material as a photonic detector. These types of sensors have a high detectivity D^* (around 2×10^{10} cm Hz$^{1/2}$/W) but require cooling (below 100 K) to reduce thermal noise. This increases the size, the weight and the power consumption of those infrared cameras, all factors that limit the use of this technology in portable systems. On the other hand, microbolometers sensors can be operated at room temperature. Furthermore, they are a lot less expensive to manufacture than imagers based on MCT technology since all the fabrication steps are compatible with standard CMOS technology. Two important drawbacks are their low detectivity (compared to MCT) and the fact that those sensors have to be optimized for a particular infrared band.

Optoelectronic properties of carbon nanotubes makes them very interesting component for infrared sensors [1–3]. Interest in carbon nanotubes as a photonic infrared sensors increased since the photoconductivity of a single CNT was measured [4]. A quantum efficiency of at least 10% was found. This value is lower than the quantum efficiency of HgCdTe (near 100% at the peak wavelength) but could be brought well above that of GaAs/AlGaAs quantum well IR photo-detectors (QWIPs) (around 10%). It was also shown that the response of a single nanotube can be greatly enhanced by adding a nanoantenna [5]. One of the major challenges in fabricating a photonic sensor based on carbon nanotubes is the processing required to produce a practical device that is not based on a single tube. To put this into context, a state-of-the-art MCT focal plane array typically will have 320×240 pixels with a 25 μm pitch. To fabricate a similar focal plane array, many carbon nanotubes would have to be densely packed on a 25×25 μm^2 surface to provide near 100% coverage.

Carbon nanotubes are also of interest for microbolometer applications; the very high optical absorption over a wide spectral range of this material [6] makes it a very interesting as a wideband absorber. Also, oriented CNT layers can be grown so that only the base of the tubes is in contact with the substrate, thus minimizing thermal conductivity, a feature that is of the foremost importance to maximize microbolometer response. Given that the temperature coefficient of resistance (TCR) is sufficiently high and that electrical contacts can be successfully deposited, a patterned film of oriented CNTs could then be used as a wideband microbolometer.

In order to explore the possibility of using CNTs for photonic and bolometer type infrared detectors, two different test devices were fabricated. In this paper, we present results on the infrared response of those two prototypes.

2. Experimental details

2.1. Carbon nanotubes on silicon

The general experimental conditions for the growth of carbon nanotubes have been described previously [7], but we include it here with more details. We use prime grade N-type Sb doped Si substrates with ⟨100⟩ orientation in these experiments. The TiN interlayer has a dual functionality in our sensor structure. It acts as an electrode, which provides the electrical contact for the CNTs, and it also forms a protective barrier layer against diffusion of the Ni catalyst and formation of NiSi$_x$. This silicide formation occurs at temperatures above 300 °C [8]. The TiN layer is deposited by DC-magnetron sputtering. A 99.5% pure TiN target is used and the Si substrates are heated to 500 °C for the deposition in a reactive Nitrogen atmosphere at 1.2 mTorr. A TiN thickness of 100 nm is used in our experiments. The Ni catalyst layer is then deposited by RF-magnetron sputtering using a 99.9% pure Ni target at ambient temperature under Ar atmosphere at 0.72 mTorr. Deposition parameters are set to obtain typical catalyst layer thicknesses of 10 nm. Thicknesses are measured by ellipsometry. After the deposition of TiN and Ni layers, the resulting Ni/TiN/Si material is then transferred in air into the MPECVD reactor.

The 2.45 GHz microwave generator of the MPECVD system could be operated with the power up to 1.0 kW. The H$_2$, CH$_4$ and Ar process gases were introduced independently in the chamber through electronically controlled mass flow controllers. The substrates can be heated up to 800 °C and maintained at constant temperature.

We use a synthesis procedure that includes a H$_2$ plasma pretreatment step. The pretreatment reduces NiO$_x$ and then activates the catalyst for the subsequent growth process [9]. To assure process reproducibility, the chamber is pumped to 10^{-6} Torr prior to introducing the H$_2$ gas. The substrates are gradually heated to the growth temperature of 700 °C in about 30 minutes. The temperature is kept constant for another 10 min, before the ignition of the H$_2$ plasma at 4 Torr and 900 W of microwave power. After 10 min of H$_2$ plasma pretreatment, the CH$_4$ gas is then introduced into the chamber for the CNT synthesis at 900 W. The total pressure in the chamber is maintained at 5 Torr during the 20 minutes growth process. A CH$_4$:H$_2$ ratio of 1:4 is used. Ar refilling of the chamber is performed at the end of the growth process to cool the samples down to ambient temperature. It should be noted that the substrate temperature could increase during experiment, as a result of contact with the plasma. However, these variations are identical for all samples. Carbon nanotubes layer produced using this method are 10 μm thick, dense and vertically aligned. The nanotubes themselves are multi-wall with a diameter of about 20 nm.

In order to process the resulting film, the carbon nanotubes were encased into polyimide (PI-2737 from HD Microsystems). To achieve this, first, the polyimide solution is applied on the nanotube layer, enough to entirely cover the tubes. A soft-bake is then performed at 55 °C for 75 minutes. The sample is later cured at 350 °C for 60 minutes in nitrogen. After
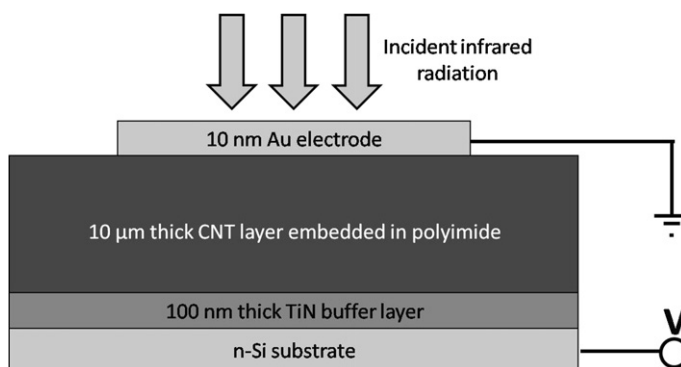
Fig. 1. Representation of the carbon nanotube device on silicon.

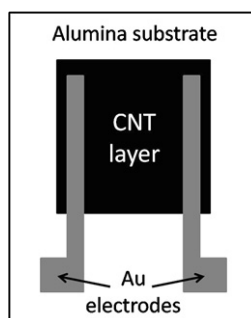**Fig. 1.** Schéma du dispositif à base de nanotubes de carbone sur silicium.

Fig. 2. Representation of the carbon nanotube device on alumina.

Fig. 2. Schéma du dispositif à base de nanotubes de carbone sur alumine.

those heat treatments, the polyimide is mechanically polished, exposing the tip of the nanotubes, before the deposition of a 10 nm thick gold electrode by vacuum evaporation. The gold film is deposited through a shadow mask, defining a 5 mm × 5 mm square. Fig. 1 presents the structure of the device.

2.2. Carbon nanotubes on alumina

The nanotube layers on alumina substrates are grown in similar conditions except that the TiN buffer layer and the polyimide are omitted. Also, the Ni catalyst layer is deposited through a 1 cm × 1 cm shadow mask, limiting the growth to a clearly defined area. The nanotubes grown on alumina did not show vertical alignment. Gold electrodes are also deposited by vacuum evaporation through a shadow mask. Contrary to the CNT on silicon device, the electrical contact geometry is parallel to the sample surface. Fig. 2 presents the structure of the device on alumina.

3. Results and discussion

3.1. Infrared response of the CNT on silicon sample

In order to perform infrared response measurements, the device is mounted in a dewar, under vacuum, and cooled to a temperature of 100 K. A ZnSe window enables the illumination of the sample. The illumination source is a wideband glowbar located 12 cm away from the device. Fig. 3 shows the I–V curve of the CNT on silicon device with and without illumination. It can be observed that the bias voltages for which the difference in current between the dark and illuminated conditions is most evident are located between 0 and −1 V. The rise time of the device is measured using a 1.04 μm laser source, a mechanical chopper and an oscilloscope. A value of about 1 ms is found.

The spectral response of the device is measured by using a tungsten lamp in a quartz bulb as the source of illumination. The light is modulated by a mechanical chopper and feed into an infrared monochromator. The device is located at the exit slit. The response of the device is measured by a lock-in amplifier, using the reference frequency of the mechanical chopper. Fig. 4 presents the spectral response of the device. It can be observed that the peak response occurs at about 1.02 μm. This is a similar result than the one observed by Straus et al. [10]. The peak detectivity of the device is evaluated to be equal to 5×10^7 cm Hz$^{1/2}$/W. The cut-off wavelength is equal to 1.15 μm. The measured spectral response is analogous to the one of silicon. It is quite likely that the observed infrared response of the device is in fact the response of the substrate. The
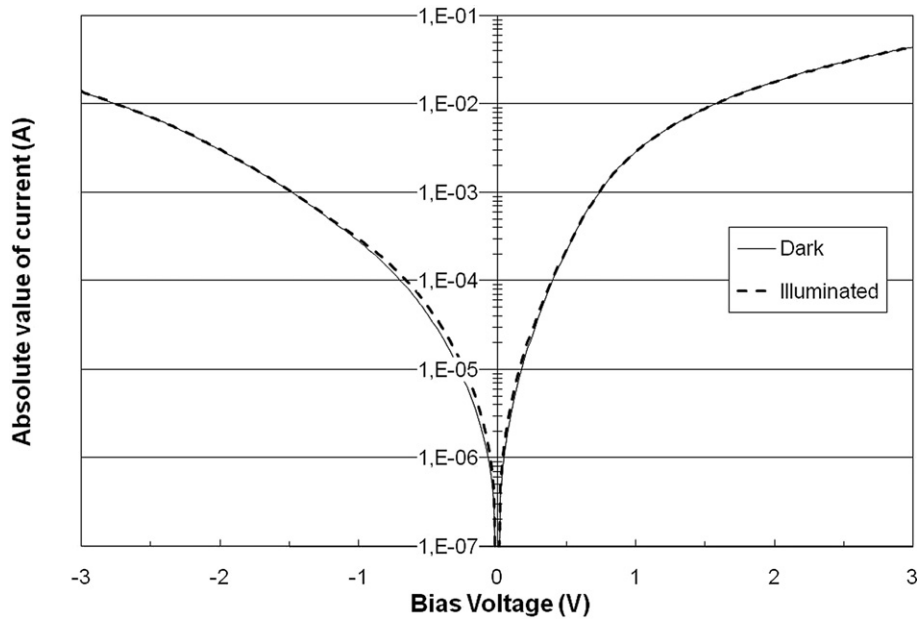
Fig. 3. Current-voltage behavior of the CNT on silicon device at a temperature of 100 K with and without illumination.
Fig. 3. Comportement courant-voltage du dispositif à base de NTC sur silicium à une température de 100 K avec et sans illumination.
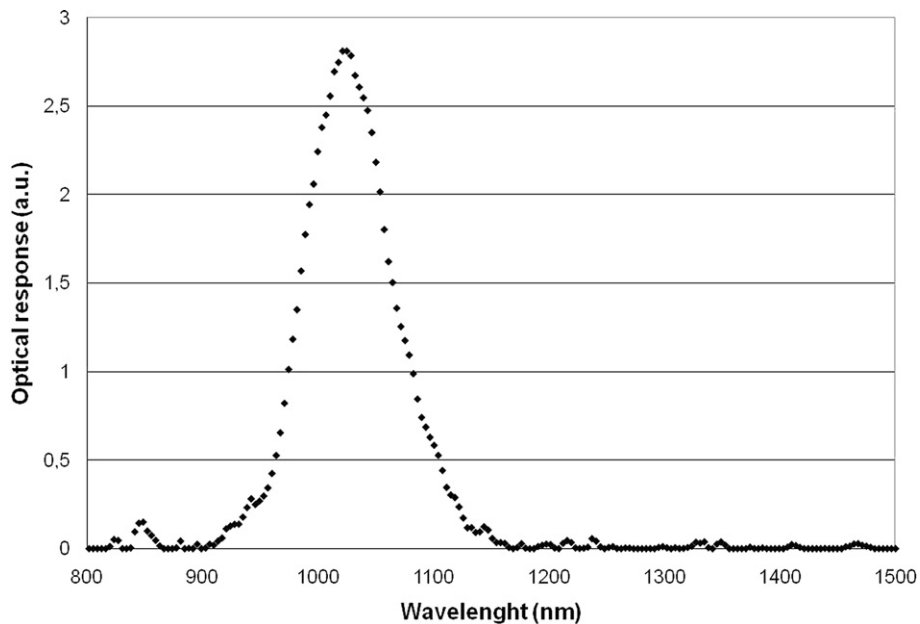

Fig. 4. Spectral response of the CNT on silicon device (bias voltage of −0.18 V).
Fig. 4. Réponse spectrale du dispositif à base de NTC sur silicium (polarisation de −0.18 V).

contribution of the CNT layer is possibly overwhelmed. To isolate the specific infrared detection of the carbon nanotubes, another configuration must be used. This is what is presented in the next section.

3.2. Infrared response of the CNT on alumina sample

Fig. 5 presents the temperature coefficient of resistance (TCR) as a function of the temperature of the sample. The absolute value of TCR is below 0.15%/K at a temperature of 300 K. If the sample is cooled to 100 K, the TCR increases to 0.42%/K. This is lower that what can be measured for YBCO films, which can have absolute TCR values in excess of 2.5%/K at room temperature [11].

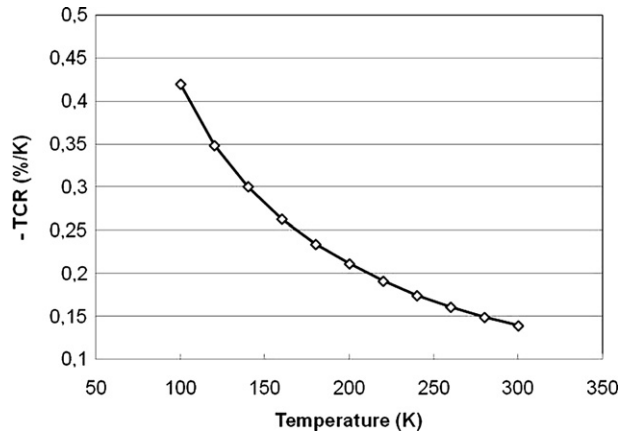**Fig. 5.** Temperature coefficient of resistance as a function of temperature for the CNT on alumina device.

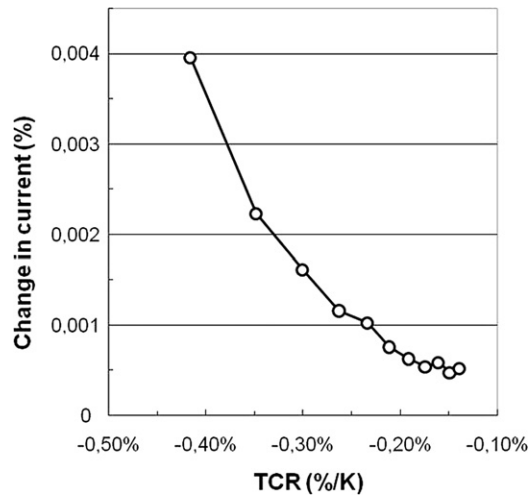**Fig. 5.** Coefficient thermique de résistance en fonction de la température pour le dispositif à base de NTC sur alumine.

Fig. 6. Infrared induced variation of current as a function of the temperature coefficient of resistance.

Fig. 6. Variation du courant induite par le rayonnement infrarouge en fonction du coefficient thermique de résistance.

The infrared response of the sample is also measured under vacuum and different temperatures using a wideband glow-bar. To examine the role of the TCR values on the infrared response, the variation in current induced by infrared illumination is plotted as a function of TCR (see Fig. 6). If all parameters stay constant, we would expect a linear relation if the detection mechanism was a bolometric effect. This is what is observed in Fig. 6 even though the linear relation is not perfect. The TCR is one important factor in the response of a bolometer, another crucial parameter is the thermal conduction of the active element with the substrate. This last parameter could also change with temperature, thus explaining some of the non-linearity. The fact that the detection mechanism is thermal is consistent with the long response time measured which is in the order of the second.

Using optical filters, it is found that the sample responds to radiation in the visible, mid-wave and long-wave infrared bands, which is expected since the CNT layer should have a broad absorption spectral range. Also, the overall detectivity is equal to about 6000 cm Hz$^{1/2}$/W. Obviously, this is much lower than state-of-the art VO$_2$ or amorphous silicon microbolometers arrays which have detectivity values in excess of 10^8 cm Hz$^{1/2}$/W, but it should not be seen as an upper limit on the performance of this approach since very little optimization is performed in this study.

4. Conclusions

Multi-wall carbon nanotube layers were grown on silicon and alumina to explore strategies for the fabrication and characterization of infrared sensors based on this material. A CNT on silicon device was successfully fabricated using conventional micro-fabrication methods. The I–V curve and the spectral response were also measured. For the carbon nanotube layer on alumina, the temperature coefficient of resistance of the nanotubes was evaluated. The infrared response was found to be consistent with a bolometric effect. Also, the device showed a wide spectral response. For future work, it would be

interesting to produce vertically aligned layers of single-wall carbon nanotubes and characterize the infrared response of a device incorporating this material.

Acknowledgements

References

[1] J.M. Xu, Infr. Phys. Tech. 42 (2001) 485–491.
[2] J.W.G. Wildoer, L.C. Venema, A.G. Rinzler, R.E. Smally, C. Dekker, Nature 391 (1998) 59–62.
[3] T.W. Odom, J. Huang, P. Kim, C.M. Lieber, Nature 391 (1998) 62–64.
[4] M. Freitag, Y. Martin, J.A. Misewich, R. Martel, Ph. Avouris, Nano Lett. 3 (2003) 1067–1071.
[5] C.K.M. Fung, N. Xi, B. Shanker, K.W.C. Lai, Nanotechnology 20 (2009) 185201 (6 pp).
[6] Z.-P. Yang, L. Ci, J.A. Bur, S.-Y. Lin, P.M. Ajayan, Nano Lett. 8 (2008) 446–451.
[7] J.-B.A. Kpetsu, P. Jedrzejowski, C. Côté, A. Sarkissian, P. Mérel, P. Laou, S. Paradis, S. Désilets, H. Liu, X. Sun, Nanoscale Res. Lett. 5 (2010) 539–544.
[8] M. Chhowalla, K. Teo, C. Ducati, N.L. Rupesinghe, G. Amaratunga, A.C. Ferrari, D. Roy, J. Robertson, W.I. Milne, J. Appl. Phys. 90 (2001) 5308–5317.
[9] J.H. Yen, I.C. Leu, C.C. Lin, M.H. Hon, Diamond and Related Materials 13 (2004) 1237–1241.
[10] A.D. Straus, M. Tzolov, T.-F. Kuo, A. Yina, D.A. Cardimona, J.M. Xua, Proc. SPIE 6308 (2006) 63080Q1–63080Q8.
[11] P. Mérel, P. Laou, F. Wong, Proc. SPIE 5783 (2005) 607–617.